




Cite this: *RSC Adv.*, 2020, 10, 34775

# A facile method for the preparation of black TiO<sub>2</sub> by Al reduction of TiO<sub>2</sub> and their visible light photocatalytic activity

Jun Li, \* En-Hui Wu, Jing Hou, Ping Huang, Zhong Xu, Yan Jiang,  Qian-Shu Liu and Yu-Quan Zhong

Black TiO<sub>2</sub> has attracted widespread attention due to its visible light absorption and wide range of applications. However, the currently reported preparation methods for black TiO<sub>2</sub> are not suitable for large-scale production due to its being prepared under high vacuum and over a long time. We have successfully prepared black TiO<sub>2</sub> under normal pressure and short time conditions. The as-prepared black titanium dioxide was characterized by XRD, XPS, TEM, UV-visible absorption spectrum and other characterization methods. The result shows that the as prepared black titanium dioxide had a disordered structure and oxygen vacancy defects on the surface, and exhibits excellent visible and near infrared absorption performance. The black TiO<sub>2</sub> sample was prepared under 650 °C 60 min exhibits excellent visible light photocatalytic performance, and can degrade 56% MO after visible light irradiation for 120 min.

Received 13th August 2020  
Accepted 14th September 2020

DOI: 10.1039/d0ra06784a

rsc.li/rsc-advances

## 1. Introduction

TiO<sub>2</sub> has become one of the most studied photocatalyst materials since the Japanese scientists Fujishima and Honda discovered that the TiO<sub>2</sub> electrode photolyzes water.<sup>1</sup> TiO<sub>2</sub> has been widely studied for hydrogen production,<sup>2,3</sup> dye-sensitized solar cells,<sup>4,5</sup> CO<sub>2</sub> reduction,<sup>6–8</sup> environmental pollution removal,<sup>9</sup> toxic gas oxidation<sup>10</sup> and photocatalytic organic synthesis of chemicals.<sup>11</sup> However, TiO<sub>2</sub> can only absorb the energy in the ultraviolet region because the band width of TiO<sub>2</sub> is 3.0 to 3.2 eV. The solar energy utilization rate of TiO<sub>2</sub> is seriously insufficient due to the UV light area only accounting for less than 5% of sunlight. Many methods such as element doping, oxygen vacancies, dye-sensitization and preparation of composite materials have been made to improve light absorption properties of TiO<sub>2</sub> materials.<sup>12–24</sup> However, the results are not up to the mark.

Black TiO<sub>2</sub> is first produced by Chen *et al.* in 2011,<sup>25</sup> which have received widespread attention due to enhanced sunlight absorption by forming oxygen vacancies and Ti<sup>3+</sup> in TiO<sub>2</sub> or introducing a disordered layer on the surface of highly crystalline TiO<sub>2</sub>. Since then, black TiO<sub>2</sub> became an active research area for many applications which include photocatalytic pollutant degradation, hydrogen production through water splitting, photocatalytic CO<sub>2</sub> reduction, dye sensitized solar cells, lithium batteries and other photoelectrochemical applications with great success.

Currently, different strategies have been employed for the synthesis of black TiO<sub>2</sub>. The preparation methods and process conditions of common black titanium dioxide are shown in Table 1.

Hydrogenation is the widely used method for synthesizing black TiO<sub>2</sub>. Although there are many ways to prepare black titanium dioxide. However, novel green synthesis methods which are easy, low cost, fast and eco-friendly need to be further developed.

The methods for preparing black titanium dioxide described above all require high-pressure hydrogen or inert gas or vacuum conditions. The preparation conditions are relatively harsh, the equipment requirements are high and continuous preparation is very difficult, resulting in higher costs for preparing black titanium dioxide and difficult to prepare on a large scale.

In this paper, the author cleverly designed a molten B<sub>2</sub>O<sub>3</sub> covering the surface of the reaction raw materials to effectively isolate the air and B<sub>2</sub>O<sub>3</sub> can be recycled repeatedly, as shown in Fig. 1. Black titanium dioxide can be prepared under normal pressure, which does not require inert atmosphere or vacuum conditions. At the same time, this method has low reaction temperature, short reaction time and low equipment requirements. The cost of preparing black titanium dioxide can greatly reduce and easy to realize large-scale preparation. The photocatalytic activity of the synthesized black TiO<sub>2</sub> materials was also investigated by the degradation of methyl orange (MO) under the visible light irradiation.

At present, the preparation methods of black TiO<sub>2</sub> mainly include gas phase atmosphere sintering (high pressure pure hydrogen),<sup>25,26</sup> chemical reduction (aluminum reduction, magnesium reduction),<sup>27,28</sup> chemical oxidation<sup>29</sup> and

Panzhihua International Research Institute of Vanadium and Titanium, Panzhihua University, Panzhihua 617000, People's Republic of China. E-mail: lidejun163@126.com



**Table 1** The currently reported preparation process of black titanium dioxide

Number	Preparation process	Process conditions
1	High/low pressure hydrogen treatment	The black TiO <sub>2</sub> nanocrystals was synthesized in a 20 bar H <sub>2</sub> atmosphere at elevated temperatures ranges from 200 to 450 °C for few days <sup>25–27</sup>
2	Hydrogen–argon treatment	The black TiO <sub>2</sub> nanocrystals were obtained by under H <sub>2</sub> –Ar mixture at 450 °C for 1 h <sup>28</sup>
3	Argon–nitrogen treatment	The black TiO <sub>2</sub> –B nanoparticles were obtained by heating the solid product obtained in the above process at 340 °C in Ar atmosphere for 2 h <sup>29</sup> A core–shell black anatase TiO <sub>2</sub> with a high concentration of Ti <sup>3+</sup> and oxygen vacancy defects by a one-pot synthetic method calcination of colloidal TiO <sub>2</sub> precursor under N <sub>2</sub> atmosphere alone <sup>30</sup>
4	Hydrogen nitrogen treatment	Black TiO <sub>2</sub> through hydrogen spill in a H <sub>2</sub> –N <sub>2</sub> atmosphere at 200–700 °C <sup>31</sup>
5	Argon treatment	The black TiO <sub>2</sub> precursor (Ni doped TiO <sub>2</sub> ) was mixed with 2 g of NaBH <sub>4</sub> and heated at 350 °C under Ar atmosphere for 1 h <sup>32</sup>
6	Plasma treatment	Precursor TiO <sub>2</sub> was subjected to heat at 350–500 °C for 3 h under the hot filament (2000 °C) resulted in black colored TiO <sub>2</sub> nanotubes <sup>33</sup>
7	NaBH <sub>4</sub> reduction	P25 (anatase and rutile) was ground thoroughly with NaBH <sub>4</sub> and the mixture was heated in a tubular furnace under Ar atmosphere at 300–400 °C for different time intervals up to 1 h <sup>34</sup>
8	Metal reduction	Black TiO <sub>2</sub> nanoparticles could be synthesized through reduction with various metals. Aluminum <sup>35</sup> and magnesium <sup>36</sup> are identified as reducing agents to obtain black TiO <sub>2</sub> . Wang <i>et al.</i> used Al as a reducing agent in an evacuated two-zone vacuum furnace at 300 to 50 °C. In a typical procedure, pre-annealing of aluminum was done at 800 °C for 6 h and that of pristine TiO <sub>2</sub> was done at 500 °C for 20 h respectively. Further the post annealing was carried out at 800 and 900 °C for 12 h respectively <sup>37</sup>

electrochemical reduction.<sup>30</sup> However, these preparation methods are not suitable for large-scale production due to their high cost. Therefore, it is of great significance to seek a simple, efficient and low-cost method for preparing black titanium dioxide.

In this paper, a novel method for preparation of black TiO<sub>2</sub> by aluminothermic reduction had been studied. Through clever design, black TiO<sub>2</sub> materials has been successfully prepared at a lower calcination temperature and a shorter time under normal pressure. The photocatalytic activity of the synthesized black TiO<sub>2</sub> materials was also investigated by the degradation of methyl orange (MO) under the visible light irradiation.

## 2. Experimental

### 2.1 Preparation of black TiO<sub>2</sub>

Anatase type TiO<sub>2</sub> (typically 0.4–0.6 μm in diameter) were purchased from Sichuan province excellence vanadium and titanium Co., Ltd. Aluminum powder (99.3% purity, 6 μm particle size) were purchased from Jiangsu tian yuan metal powder co., Ltd. Firstly, the anatase TiO<sub>2</sub> powder mixed with Al powder was placed in alumina crucible. Secondly, an aluminum sheet as large as the corundum crucible was placed on the surface of the mixed raw material and then a layer of molten B<sub>2</sub>O<sub>3</sub> was covered the surface of the aluminum sheet so as to isolate the raw material from air contact. Thirdly, corundum crucible was roasted in a resistance furnace. Finally, hydrochloric acid pickling method was used to remove excess Al from the as-prepared sample. The prepared sample was mixed with hydrochloric acid in a beaker at a stirring rate of 100 rpm, and it was filtered using a vacuum suction funnel after the reaction was completed. The concentration of hydrochloric acid was

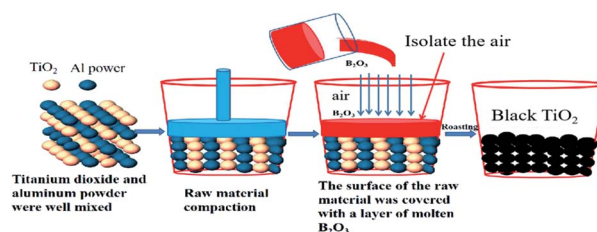
4 mol L<sup>−1</sup> and the liquid–solid ratio was 1 : 25. The preparation process of black titanium dioxide was shown in Fig. 2.

### 2.2 Photocatalytic activity test

Photocatalytic activity of the synthesized black TiO<sub>2</sub> powders by the degradation of methylene orange (MO) under a 300 W xenon lamp equipped with a cutoff filter (λ > 420 nm). A quantity of 100 mg of photocatalyst was poised in a 200 mL aqueous MO dye solution (0.5 g L<sup>−1</sup>). Previous to the light, the suspensions were ultrasonicated for 25 min under dark condition to make sure that the MO dye was adsorbed to saturation level on the surface of catalysts.

### 2.3 Sample characterization

Powder X-ray diffraction (XRD) profiles were obtained using a D/max22500PC of Japanese Science and Technology with Cu Kα (λ = 0.154 nm) radiation as the incident beam. Transmission electron microscopy (TEM) was performed on a Hitachi H-9000 instrument operating at 300 kV. Scanning electron microscopy (SEM) was performed on JEOL JSM-6060S and JSM-6700F

**Fig. 1** Schematic diagram of roasting stage.

instruments. XPS profiles were obtained using Phi-5000 VersaProbe of America.

### 3. Results and discussion

#### 3.1 XRD and Raman analysis of samples

Black TiO<sub>2</sub> materials were successfully synthesized using an Al reduction process. Commercial anatase TiO<sub>2</sub> power (50 g) were uniformly mixed with 30 g of Al powder, and then calcined at 650 °C for 60 min, 90 min, 120 min, 150 min. The pure TiO<sub>2</sub> were then obtained after excess Al was removed by pickling with hydrochloric acid and distilled water.

Macro picture of experimental results is depicted in Fig. 3(a). The color of anatase titanium dioxide starts to change from white to black at 650 °C for 60 min. The XRD patterns of the raw material and as-prepared samples are shown in Fig. 2(a). The prepared black TiO<sub>2</sub> has good crystallinity, and its characteristic peaks match well with anatase TiO<sub>2</sub> without any other diffraction peaks. The characteristic peak of the (101) plane of black TiO<sub>2</sub> shifts to the right small diffraction angle and the larger the diffraction angle shifts to the right as the sintering time increases, which may be due to certain lattice defects.<sup>38</sup> In addition, the half peak width of as-prepared black TiO<sub>2</sub> is wider comparing with anatase TiO<sub>2</sub>, which indicate that the degree of crystallinity of as-prepared black TiO<sub>2</sub> is poor compared with anatase TiO<sub>2</sub> and the crystal size of as-prepared is smaller than the anatase TiO<sub>2</sub>.

Fig. 3(b) shows the Raman spectrum of the raw material and as-prepared samples. The strongest intensity Raman active mode at 144 cm<sup>-1</sup> and three medium intensity Raman active modes at 394 cm<sup>-1</sup>, 515 cm<sup>-1</sup>, and 636 cm<sup>-1</sup> were detected in all the samples, which match well with anatase TiO<sub>2</sub>. The as-prepared black TiO<sub>2</sub> confirmed the presence of oxygen vacancies defects because the strongest E<sub>g</sub> mode at 144 cm<sup>-1</sup> broadening and blue shift compared with that of pristine anatase TiO<sub>2</sub>.

#### 3.2 X-ray photoelectron spectroscopy (XPS) analysis of samples

Valence band position and useful information of chemical binding on the sample surface can be provided by X-ray photoelectron spectroscopy (XPS). Fig. 4(a–d) shows the Ti2p and O1s core level XPS spectra of the pristine TiO<sub>2</sub> and as-

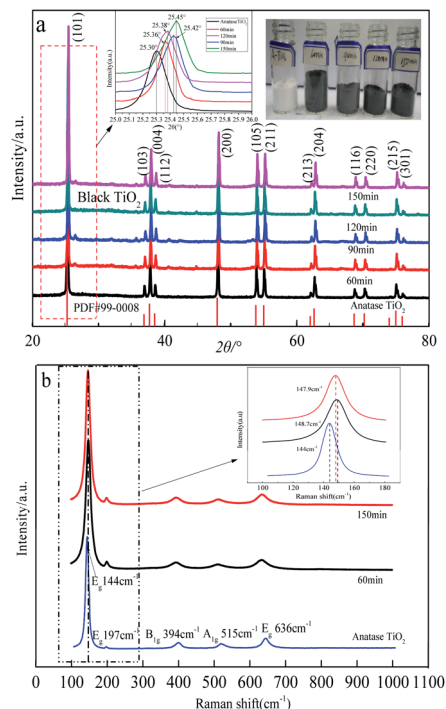


Fig. 3 XRD and Raman analysis of samples. (a) XRD and macro pictures of samples; (b) Raman spectrum of the samples.

prepared black TiO<sub>2</sub>. Fig. 3(a) shows the Ti2p XPS spectra of anatase TiO<sub>2</sub> and black TiO<sub>2</sub>. The two Ti2p peaks of anatase TiO<sub>2</sub> and black TiO<sub>2</sub> were located at 458.6 eV and 464.4 eV match well with Ti<sup>4+</sup> in TiO<sub>2</sub>.<sup>39</sup> However, the significant Ti<sup>3+</sup> signal could not be detected in the black TiO<sub>2</sub>. The possible reason is that Ti<sup>3+</sup> didn't appear in the crystal lattice, but it plays

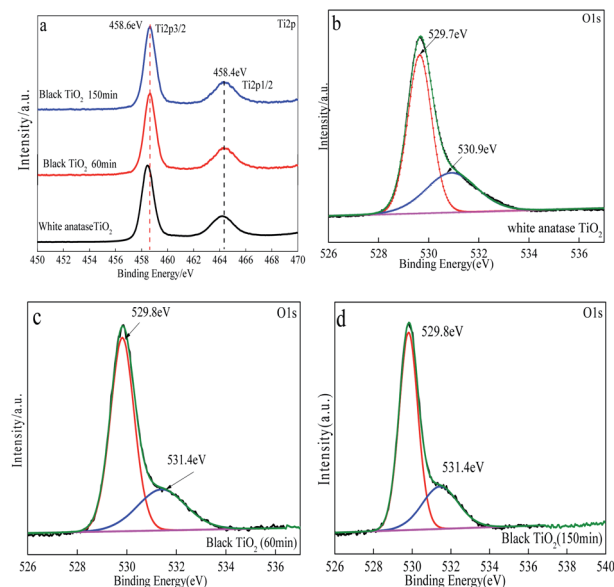


Fig. 4 XPS analysis of the samples. (a) Ti2p core level XPS spectra of the TiO<sub>2</sub> and black TiO<sub>2</sub>; (b–d) O1s core level XPS spectra of the TiO<sub>2</sub> and black TiO<sub>2</sub>.

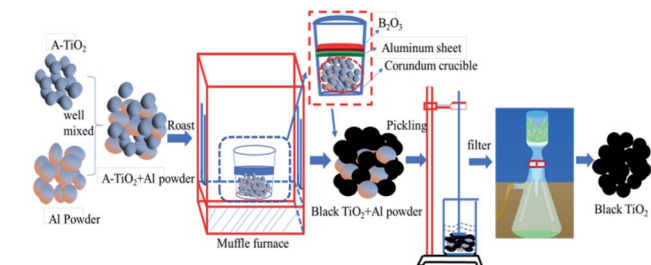


Fig. 2 Schematic diagram of black titanium dioxide was synthesized by aluminothermic reduction and hydrochloric acid pickling.



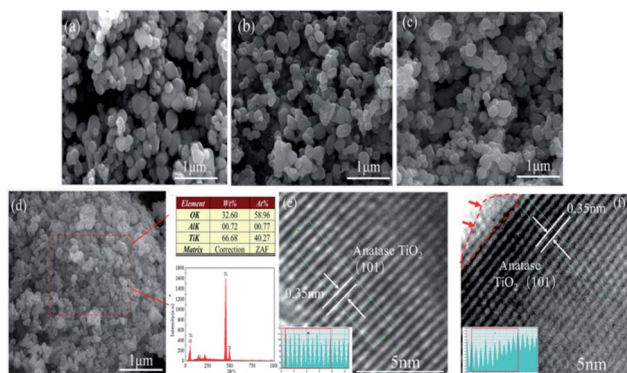


Fig. 5 SEM, EDS and HR-TEM analysis of samples. (a)–(c) SEM images of pristine TiO<sub>2</sub> and as-prepared black TiO<sub>2</sub> (650 °C, 60 min and 650 °C, 150 min); (d) EDS analysis of the black TiO<sub>2</sub> was pickled by hydrochloric acid; (e) and (f) HR-TEM image of the TiO<sub>2</sub> and black TiO<sub>2</sub>.

an important role in color change.<sup>40</sup> The O1s XPS spectra of the pristine TiO<sub>2</sub> and black TiO<sub>2</sub> are depicted in Fig. 3(c and d). The peak for O1s could be deconvoluted into two peaks at about 529.7 eV and 530.9 eV. The peaks at 529.7 eV in anatase TiO<sub>2</sub> and black TiO<sub>2</sub> were belong to the crystal lattice of the Ti–O bond, while the peaks at 530.9 eV or 531.4 eV were the external –OH group or H<sub>2</sub>O molecules absorbed on the anatase TiO<sub>2</sub> and black TiO<sub>2</sub> surface.<sup>41</sup> It was clearly seen that –OH group absorption intensity of black TiO<sub>2</sub> was significantly higher than that of anatase TiO<sub>2</sub> due to the presence of oxygen vacancies in the black TiO<sub>2</sub>.

### 3.3 SEM, EDS and HR-TEM analysis of samples

Fig. 5(a–c) shows SEM images of pristine TiO<sub>2</sub> and black TiO<sub>2</sub>, respectively. Pristine TiO<sub>2</sub> with a particle size of 200–300 nm, and the morphology of black TiO<sub>2</sub> had not obvious sintering growth compared to pristine anatase TiO<sub>2</sub>. The EDS analysis (Fig. 4(d)) shows only trace amounts of Al in black TiO<sub>2</sub>.

The morphology and structure of pristine TiO<sub>2</sub> and as-prepared black TiO<sub>2</sub> were further examined by TEM. Fig. 5(e and f) shows HR-TEM analysis of pristine TiO<sub>2</sub> and black TiO<sub>2</sub>. A lattice space of as-prepared black TiO<sub>2</sub> and pristine TiO<sub>2</sub> were 0.35 nm, which were well-resolved (101) lattice plane of typical anatase TiO<sub>2</sub> plane. Both HR-TEM and XRD analysis results indicate that the as-prepared black TiO<sub>2</sub> contains a pure anatase phase. The area was marked by the red arrow in Fig. 4(f) could be seen that the as-prepared black TiO<sub>2</sub> contained an outer disordered structure on the surface compared to pristine anatase TiO<sub>2</sub>.

### 3.4 UV-Vis diffuse reflectance spectroscopy analysis of samples

UV-Vis diffuse reflectance spectroscopy are used to evaluate the light absorption characteristics of the sample. The UV-Vis diffuse reflectance spectra is depicted in Fig. 6(a) shows the as-prepared black TiO<sub>2</sub> exhibits excellent visible and near infrared absorption performance, and anatase TiO<sub>2</sub> mainly absorb ultraviolet light. It can be clearly seen that the UV-visible

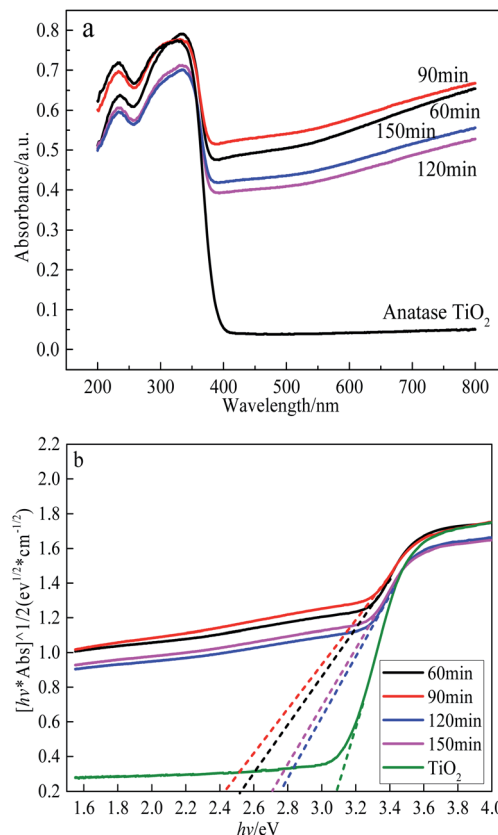


Fig. 6 UV-Vis diffuse reflectance spectroscopy analysis. (a) UV-Vis diffuse reflectance spectroscopy of the TiO<sub>2</sub> and black TiO<sub>2</sub>; (b) plots of  $(ah\nu)^{1/2}$  versus photon energy ( $h\nu$ ).

spectrum of as-prepared black TiO<sub>2</sub> occurred a red shift comparing with white anatase TiO<sub>2</sub>. Kubelka Munk function formula ( $\alpha h\nu = C(h\nu - E_g)^{1/2}$ ) could be used to calculate the band gap of semiconductor materials based on UV-Vis DRS, as shown in Fig. 6(b). It can be seen that the band gap of the prepared black TiO<sub>2</sub> was 2.4–2.8 eV, which was significantly narrowed compared with white TiO<sub>2</sub> (3.1 eV). The band gap of black TiO<sub>2</sub> was narrowed and the absorption spectrum expand to the visible light scope may be caused by Ti dangling bonds was related with oxygen vacancy defects.<sup>42</sup>

### 3.5 Photocatalytic activity analysis of samples

The photocatalytic activities of black TiO<sub>2</sub> samples were evaluated by the decomposition of MO under visible light irradiation (>420 nm), as shown in Fig. 7(a). For comparison, pure anatase TiO<sub>2</sub> was also tested under the same conditions, which can only degrade 5% MO within 120 min, respectively. The as-prepared black TiO<sub>2</sub> sample (650 °C, 60 min) could degrade 56% MO after reaction for 120 min under visible light. However, the prepared black TiO<sub>2</sub> (650 °C, 150 min) only degradation degrade 25% MO, which proves that extending the roasting time couldn't promote the visible light photocatalytic performance.

The kinetic curves for the MO photodegradation were calculated according to the equation ( $\ln(C_0/C) = kt$ ) and then plotted and displayed in Fig. 7(b). The order of photocatalytic





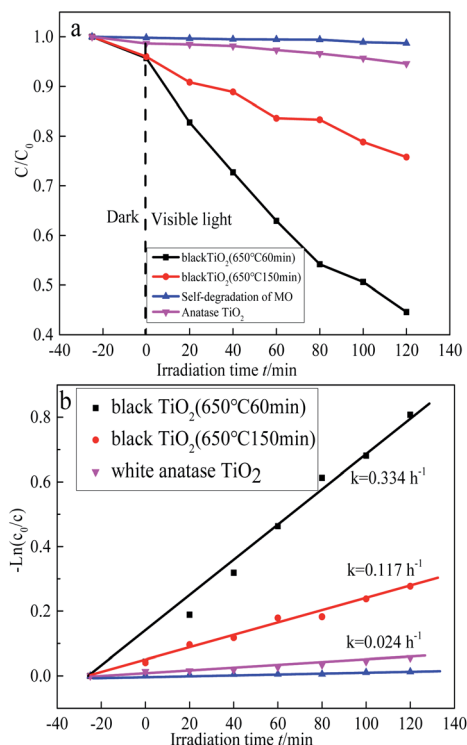


Fig. 7 Photocatalytic activity analysis of samples. (a) Photocatalytic activity of  $\text{TiO}_2$  and black  $\text{TiO}_2$  for the MO degradation under visible light irradiation; (b) kinetic curves for the MO photodegradation over black  $\text{TiO}_2$  and  $\text{TiO}_2$ .

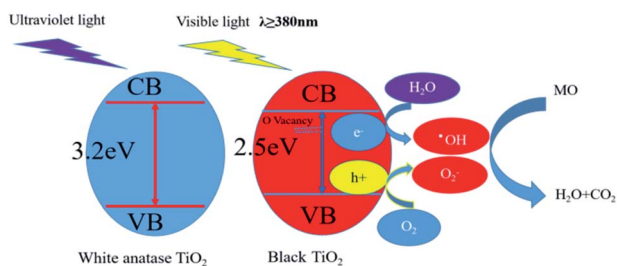


Fig. 8 Proposed mechanism for the MO degradation on the as-prepared black  $\text{TiO}_2$  photocatalyst under visible light irradiation.

performance of as-prepared photocatalysts is black  $\text{TiO}_2$  (650 °C, 60 min) > black  $\text{TiO}_2$  (650 °C, 150 min) > pure anatase  $\text{TiO}_2$ , based on the  $k$  values.

### 3.6 Mechanism analysis and discussion

High absorption of visible-light and pollutants, and a lower electron/hole recombination rate can remarkably enhance the photocatalysis. A schematic illustration of the mechanism of enhanced photocatalytic performance of as-prepared black  $\text{TiO}_2$  is shown in Fig. 8.

XRD, XPS, Raman, UV-Vis characterizations show that the prepared black titanium dioxide has formed a large number of oxygen vacancies. The presence of oxygen vacancies can reduce the recombination of electron-hole pairs and enhance visible

light absorption by moving the top of VB upward and the bottom of CB downward, respectively, resulting in black  $\text{TiO}_2$  having excellent visible light photocatalytic activity.<sup>43</sup>

Although the prepared black  $\text{TiO}_2$  enhances visible light absorption, its photocatalytic activity under visible light is still unsatisfactory due to the short lifetime of electrons and holes excited by visible light. In order to overcome this bottleneck, as-prepared black  $\text{TiO}_2$  with a series of non-metal dopants (H, S, N and I) to increase photocatalytic activities under both UV and visible-light irradiations.<sup>44</sup>

## 4. Conclusion

In this study, the black  $\text{TiO}_2$  had been successfully synthesized by aluminothermic reduction and hydrochloric acid pickling. Compared with other preparation methods, this preparation method was suitable for large-scale production because it can be prepared at a lower calcination temperature and shorter calcination time under normal pressure conditions.

The surface of as-prepared black titanium dioxide had disorder structure and oxygen vacancy defects. The particles of prepared black titanium dioxide had no obvious sintering growth, which maintains the original appearance of raw titanium dioxide. The band gap of the prepared black  $\text{TiO}_2$  are 2.4–2.8 eV, which exhibits excellent visible and near infrared absorption performance. The black  $\text{TiO}_2$  sample was prepared under 650 °C, 60 min demonstrates the highest photocatalytic activity, which can degrade 56% MO after visible light irradiation for 120 min. The products show excellent visible photocatalytic activity for dye degradation, which shows the good application value in water cleaning.

## Conflicts of interest

There are no conflicts to declare.

## Acknowledgements

This study was financially supported by the Science and Technology Support Program of Sichuan (2020YFH0195), the high-end talent introduction project of Sichuan (SYZ202006) and the Application and Solar Technology Integration Sichuan Provincial Key Laboratory of University Program (TYNSYS-2018-Z-02).

## References

- 1 A. Fujishima and K. Honda, *Nature*, 1972, **238**, 37–38.
- 2 Ni, M. K. H. Leung, D. Y. C. Leung and K. Sumathy, *Renewable Sustainable Energy Rev.*, 2007, **3**, 401–425.
- 3 J. Schneider, M. Matsuoka, M. Takeuchi, J. Zhang, Y. Horiuchi, M. Anpo and D. W. Bahnemann, *Chem. Rev.*, 2014, **19**, 9919–9986.
- 4 K. H. Park, D. W. Park and M. Dhayal, *Electrochem. Commun.*, 2008, **7**, 1098–1100.
- 5 X.-D. Li, D. W. Zhang, X. J. Yin, S. Chen, J.-H. Shi, Z. Sun and S.-M. Huang, *J. Solid State Electrochem.*, 2011, **6**, 1271–1277.



- 6 A. Corma and H. Garcia, *J. Catal.*, 2013, **4**, 168–175.
- 7 K. Kočí, L. Obalová and Z. Lacný, *Nephron Clin. Pract.*, 2008, **1**, 1–9.
- 8 J. Low, B. Cheng and J. Yu, *Appl. Surf. Sci.*, 2016, **392**, 658–686.
- 9 R. S. Dariani, A. Esmaeili, A. Mortezaali and S. Dehghanpour, *Optik*, 2016, **18**, 7143–7154.
- 10 Alonso-Tellez, D. Robert, V. Keller and N. Keller, *Environ. Sci. Pollut. Res.*, 2014, **5**, 3503–3514.
- 11 N. Kazuya and A. Fujishima, *J. Photochem. Photobiol., C*, 2012, **3**, 169–189.
- 12 X.-J. Lu, X.-L. Mou, J.-J. Wu and D.-W. Zhang, *Adv. Funct. Mater.*, 2010, **3**, 509–515.
- 13 S. Ding, X. Yin, X.-J. Lu, Y. Wang and D. Wan, *ACS Appl. Mater. Interfaces*, 2011, **1**, 306–311.
- 14 R. Ghosh, Y. Hara, L. Alibabaei, K. Hanson, S. Rangan, R. Bartynski, T. J. Meyer and R. Lopez, *ACS Appl. Mater. Interfaces*, 2012, **9**, 4566–4570.
- 15 M. Anpo, Y. Ichihashi, M. Takeuchi and H. Yamashita, *Res. Chem. Intermed.*, 1998, **2**, 143–149.
- 16 H. Irie, Y. Watanabe and K. Hashimoto, *J. Phys. Chem. B*, 2003, **23**, 5483–5486.
- 17 Y. Choi, T. Umabayashi and M. Yoshikawa, *J. Mater. Sci.*, 2004, **5**, 1837–1839.
- 18 M. Shen, Z. Wu and H. Huang, *Mater. Lett.*, 2006, **5**, 693–697.
- 19 R. Asahi, T. Morikawa, T. Ohwaki, K. Aoki and Y. Taga, *Science*, 2001, **293**, 269–271.
- 20 L. Torbjörn, J. M. Mwabora and J. Avendaño, *J. Phys. Chem. B*, 2007, **24**, 5709–5716.
- 21 L. Jia, C. Wu and Y. Li, *Appl. Phys. Lett.*, 2011, **98**, 2815.
- 22 K.-Z. Qi, B. Cheng, J.-G. Yu and W.-K. Ho, *Chin. J. Catal.*, 2017, **12**, 1936–1955.
- 23 L.-Y. Lu, G.-H. Wang and M. Zou, *Appl. Surf. Sci.*, 2018, **441**, 1012–1023.
- 24 J. Wang, G.-H. Wang and X. Wang, *Carbon*, 2019, **149**, 618–626.
- 25 X. Chen, L. Liu, P.-Y. Yu and S. S. Mao, *Science*, 2011, **331**, 746–750.
- 26 T. Leshuk, R. Parviz, P. Everett, H. Krishnakumar, R. A. Varin and F. Gu, *ACS Appl. Mater. Interfaces*, 2013, **5**, 1892.
- 27 H. Lu, B. Zhao, R. Pan, J. Yao, J. Qiu, L. Luo and Y. Liu, *RSC Adv.*, 2014, **4**, 1128.
- 28 Z. Lu, C.-T. Yip, L. Wang, H. Huang and L. Zhou, *ChemPlusChem*, 2012, **77**, 991.
- 29 L. Li, Y. Chen, S. Jiao, Z. Fang, X. Liu, Y. Xu, G. Pang and S. Feng, *Mater. Des.*, 2016, **100**, 235.
- 30 S. Wei, R. Wu, X. Xu, J. Jian, H. Wang and Y. Sun, *Chem. Eng. J.*, 2016, **299**, 120.
- 31 Y. Zhu and D. Liu, *Chem. Commun.*, 2014, **50**, 6049.
- 32 H. Zhang, Z. Xing, Y. Zhang, Z. Li, X. Wu, C. Liu, Q. Zhu and W. Zhou, *RSC Adv.*, 2015, **5**, 107150.
- 33 F. Teng, M. Li, C. Gao, G. Zhang, P. Zhang, Y. Wang and E. Xie, *Appl. Catal., B*, 2014, **148**, 339.
- 34 Q. Kang, J. Cao, Y. Zhang, L. Liu, H. Xu and J. Ye, *J. Mater. Chem. A*, 2013, **1**, 5766.
- 35 Z. Wang, C.-Y. Yang, T.-Q. Lin, H. Yin, P. Chen, D.-Y. Wan, F.-F. Xu, F.-Q. Huang, J.-H. Lin, X.-M. Xie and M.-H. Jiang, *Energy Environ. Sci.*, 2013, **10**, 3007.
- 36 Ye, J. Jia, Z.-J. Wu, C.-X. Qian, R. Chen, P. G. O. Brien, W. Sun, Y.-C. Dong and G. A. Ozin, *Adv. Energy Mater.*, 2017, **4**, 1601811.1–1601811.7.
- 37 H. Tan, Z. Zhao, M. Niu, C. Mao, D. Cao, D. Cheng, P. Feng and Z. Sun, *Nanoscale*, 2014, **6**, 10216.
- 38 R. K. Singhal, S. Kumar, P. Kumari, Y. T. Xin and E. Saitovitch, *Appl. Phys. Lett.*, 2011, **9**, 092510.1–092510.3.
- 39 W. Jiao, L. Wang, G. Liu, G.-Q. Lu and H.-M. Cheng, *ACS Catal.*, 2012, **9**, 1854–1859.
- 40 Z. Zhang, X. Tan, T. Yu, L. Jia and X. Huang, *Int. J. Hydrogen Energy*, 2016, **27**, 11634–11643.
- 41 Z. Tong, D. Yang, T. Xiao, Y. Tian and Z. Jiang, *Chem. Eng. J.*, 2015, **260**, 117–125.
- 42 L.-J. Han, B. Su, G. Liu, Z. Ma and X. An, *Mol. Catal.*, 2018, **456**, 96–101.
- 43 Wang, S. Shen and S. S. Mao, *J. Materiomics*, 2017, **2**, 96–111.
- 44 T.-Q. Lin, C.-Y. Yang, Z. Wang, H. Yin, X.-J. Lü, F.-Q. Huang, J.-H. Lin, X.-M. Xie and M.-H. Jiang, *Energy Environ. Sci.*, 2014, **3**, 967.

